ISIJ International, Vol. 55 (2015), No. 5, pp. 1067–1075

Non-linear Deformation Behavior during Unloading in Various Metal Sheets

Takayuki HAMA,* Ryogo MATSUDAI, Yota KUCHINOMACHI, Hitoshi FUJIMOTO and Hirohiko TAKUDA

Graduate School of Energy Science, Kyoto University, Yoshida-Honmachi, Sakyo-ku, Kyoto, 606-8501 Japan.

(*Received on December 15, 2014; accepted on January 26, 2015*)

The deformation behavior during unloading was examined under uniaxial tension in a mild steel sheet (body-centered cubic metal), an aluminum alloy sheet (face-centered cubic metal), and a magnesium alloy sheet (hexagonal close packed metal). A crystal plasticity finite-element method was also used to investigate the difference in the deformation behavior among on the materials. The nonlinearity during unloading was the largest in the magnesium alloy sheet, and the mild steel sheet showed a larger nonlinearity than the aluminum alloy sheet. On the other hand, the apparent elastic moduli determined from the linear approximation of unloading curves were not always consistent with the characteristics observed in the nonlinearity, and this inconsistency became pronounced as the degree of nonlinearity increased. It was found that the degree of nonlinearity would have a strong correlation with the strain rate sensitivity, suggesting that the apparent elastic modulus was not suitable to model the unloading behavior for materials with high strain rate sensitivity. The crystal plasticity analysis demonstrated that the nonlinearity was much larger in the magnesium alloy sheet than in the other two sheets as observed in the experimental results. The simulation results suggested that one of the reasons that gave rise to the nonlinearity during unloading would be the difference in the critical resolved shear stresses among the slip systems.

KEY WORDS: unloading; mild steel sheet; aluminum alloy sheet; magnesium alloy sheet; young's modulus; instantaneous gradient; crystal plasticity analysis.

1. Introduction

Springback is one of the major defects in the press forming of metal sheets, and a lot of efforts have been made to understand and to control springback.[1–6] Nowadays a simulation using the finite-element method (FEM) is a vital technology to predict springback and to determine the forming conditions.[7–12] Because the amount of springback is governed by the stress and the resultant bending moment before unloading, it is established that an elastoplastic constitutive model plays an important role in accurate prediction of springback[13] and a lot of studies have been done to develop accurate and practical constitutive models.[*e.g.*13–17]

On the other hand, it is also recognized that springback is affected also by the deformation behavior during unloading. A nonlinear stress-strain curve is often exhibited during unloading and the gradient during unloading, *i.e.* apparent elastic modulus, decreases with the increase of the plastic strain. Cleveland and Ghosh[18] measured the nonlinear deformation during unloading in aluminum (hereafter termed as Al) alloy and high strength steel sheets and found that 10–20% error in the estimation of springback may arise if the nonlinearity during unloading is not taken into account in the simulation. They concluded that mobile dislocations during unloading would be a factor of the nonlinear behavior. Luo and Ghosh[19] investigated the deformation behavior during unloading in a DQSK steel sheet and showed that apparent elastic modulus decreases rapidly at small strains and then decreases gradually at large strains. They also proposed a physically based model to describe the variation of the modulus. Andar *et al.*[20] examined the deformation during unloading under biaxial tension in high strength steel sheets and found that the inelastic strain recovery seems to be larger under biaxial unloading than that under uniaxial unloading. Kim *et al.*[21] studied the nonlinear behavior during unloading in low and high strength steel sheets under uniaxial tension. Hamasaki *et al.*[22] investigated an appropriate definition of apparent elastic modulus during unloading suitable for accurate springback predictions in cold-rolled copper alloy sheets. The present authors[23] conducted loading-unloading tests in an AZ31 magnesium (hereafter termed as Mg) alloy sheet under various loading paths and showed that the nonlinearity during unloading is different depending on loading paths. We also depicted that the nonlinear deformation during unloading in the Mg alloy sheet can be predicted well using a crystal plasticity finite-element simulation.[24,25]

The aforementioned studies exhibited that the nonlinear deformation during unloading is observed in various metal sheets and the nonlinearity during unloading plays an important role in the springback prediction. Recently the nonlinear effects are being taken into account in the constitutive models.[15] A phenomenological model to represent the nonlin-

* Corresponding author: E-mail: hama@energy.kyoto-u.ac.jp
DOI: http://dx.doi.org/10.2355/isijinternational.55.1067

earity during unloading were also proposed.[26] Furthermore, the past studies also suggested that the nonlinear characteristics would be different depending on materials. Because mobile dislocation may be one of the factors of the nonlinear deformation,[17,18] the deformation behavior may be different distinctly depending on crystal structures, such as body-centered cubic (hereafter termed as bcc), face-centered cubic (hereafter termed as fcc), and hexagonal close packed (hereafter termed as hcp) structures. However, in most of the past studies the deformation characteristics were examined for each material independently and the results have rarely been compared among the materials.[18] Therefore, detailed differences in the nonlinearity depending on the materials are not understood yet.

In the present study, the deformation behavior during unloading under uniaxial tension is examined in detail in three different metal sheets, *i.e.* an Al alloy sheet (fcc metal), a mild steel sheet (bcc metal), and a Mg alloy sheet (hcp metal). A crystal plasticity finite-element method is also used to examine the difference in the nonlinear stress-strain response among the metal sheets.

2. Experimental Conditions

Cyclic loading-unloading tests were carried out under uniaxial tension at room temperature and the stress-strain response during unloading was investigated at various pre-strains. Hereafter the strain at which the sheet was unloaded is termed unloaded strain. Materials used in the present study were a mild steel sheet with 0.8 mm thick, a A5052 Al alloy sheet with 1.0 mm thick, and an AZ31 Mg alloy sheet with 1.0 mm thick. A JIS 13B-type of specimen was used. All specimens were machined parallel to the rolling direction. The experiment was conducted at an initial strain rate of approximately 6.67×10^{-4} s^{-1} both during loading and unloading. A strain gauge (Kyowa Electronic Instruments Co., KFEM-5-120-C1) was used to measure strains. The experimental data were recorded approximately every 10 ms. The mechanical properties obtained from a uniaxial tensile test are shown in **Table 1**.

The obtained stress-strain curves during unloading were evaluated using the apparent elastic modulus E_a, the variation of instantaneous gradient $d\sigma/d\varepsilon$, and the nondimensional energy Q_{ne}. The apparent elastic modulus E_a was calculated by linearly approximating the whole unloading curve using the least square method. The instantaneous gradient $d\sigma/d\varepsilon$ was calculated using two data points for every 100 successive points[23] or a strain increment of approximately 6.67×10^{-4}. The nondimensional energy Q_{ne} is given in the form

$$Q_{ne} = \frac{Q_{ae}}{Q_{ae}+Q_a}. \quad \text{..... (1)}$$

Q_{ae} and Q_a are schematically shown in **Fig. 1**. Q_a denotes the net energy dissipated during unloading. The denominator $Q_{ae} + Q_a$ represents the energy calculated using the stress at the beginning of unloading, σ_u, and the amount of strain recovery during unloading, $\Delta\varepsilon_u$. The stronger the nonlinearity is, the larger Q_{ne} becomes.

Table 1. Tensile properties of materials used in the present study.

	E/GPa	$\sigma_{0.2}$/MPa	F/MPa	n
Mild steel sheet	206	150	544	0.25
Al alloy sheet	70.5	95.3	420	0.29
Mg alloy sheet	42.0	169	450	0.20

* The true stress-logarithmic strain curve is approximated with $\sigma=F\varepsilon^n$ in the strain range of $0.02<\varepsilon<0.1$. E is Young's modulus and $\sigma_{0.2}$ is the 0.2% proof stress.

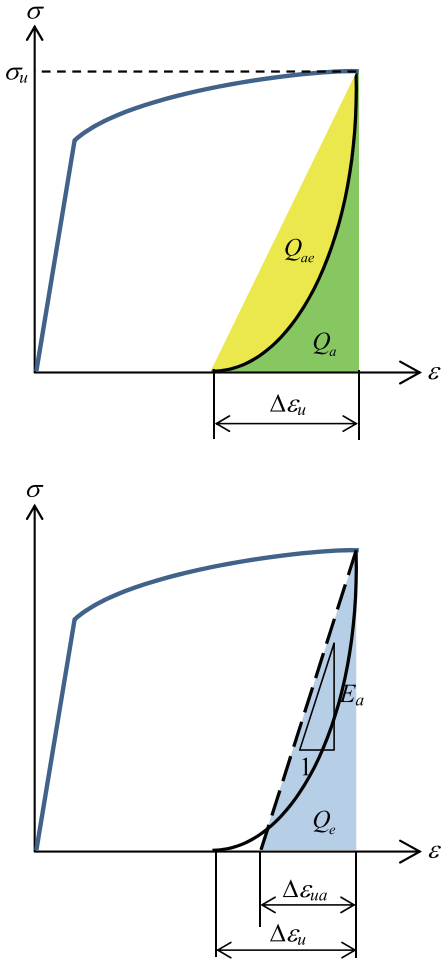

Fig. 1. Definition of energies. (Online version in color.)

3. Experimental Results and Discussion

3.1. Experimental Results

Figure 2 shows an example of the stress-strain curves during cyclic loading-unloading obtained for the three sheets. The Mg alloy sheet shows a strongly nonlinear behavior during unloading and reloading. On the other hand, the nonlinearity is much smaller in the Al alloy and mild steel sheets. To examine the nonlinearity during unloading quantitatively, an evolution of the nondimensional energy Q_{ne} as a function of unloaded strain is depicted in **Fig. 3**. Q_{ne} in the Mg alloy sheet is the largest among the three sheets and this tendency is emphasized at small unloaded strains, describing that the nonlinearity during unloading is most pronounced in the Mg alloy sheet. Q_{ne} for the mild steel sheet is larger than that of the Al alloy sheet, displaying that the nonlinearity is larger in the mild steel sheet than the Al alloy sheet.

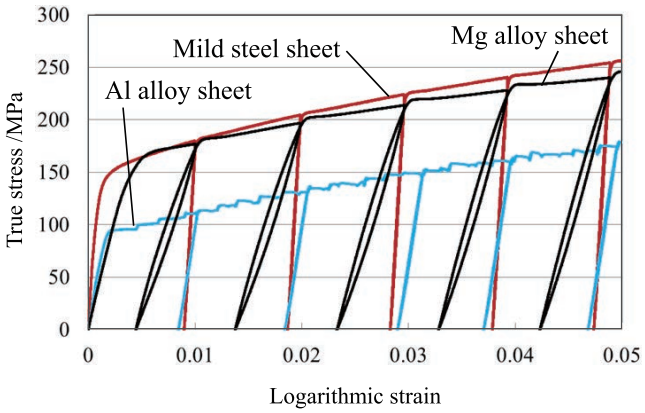

Fig. 2. Stress-strain curves during cyclic loading-unloading. (Online version in color.)

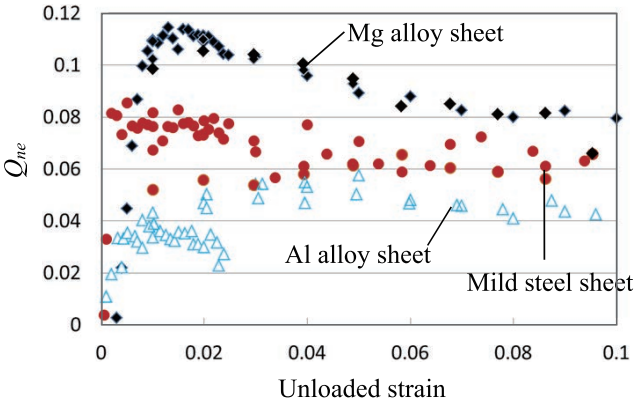

Fig. 3. Evolution of nondimensional energy Q_{ne} as a function of unloaded strain. (Online version in color.)

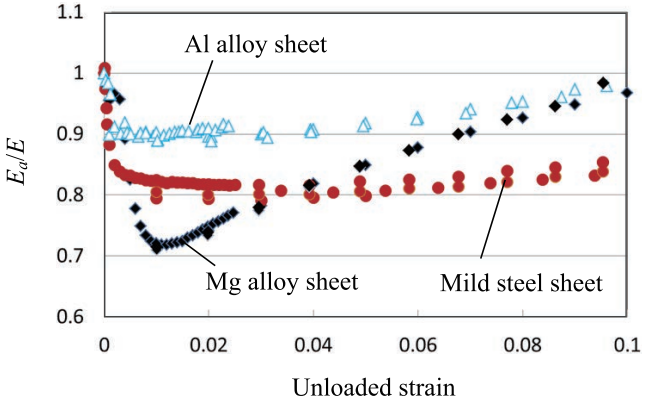

Fig. 4. Variation of apparent elastic modulus during unloading as a function of unloaded strain. (Online version in color.)

Figure 4 depicts the variations of apparent elastic modulus as a function of unloaded strain. The vertical axis is the apparent elastic modulus E_a normalized by Young's modulus E of each material. In case of the mild steel sheet, apparent elastic modulus decreases as the unloaded strain increases to approximately 0.01 and then it remains almost unchanged. This tendency is the same as that reported in the literature.[21,27] In cases of the Al alloy and Mg alloy sheets, the apparent elastic moduli decrease to unloaded strain of approximately 0.01, while they gradually increase at unloaded strains larger than approximately 0.01. The overall decrease is the smallest in the Al alloy sheet among the three sheets. On the other hand, in the Mg alloy sheet,

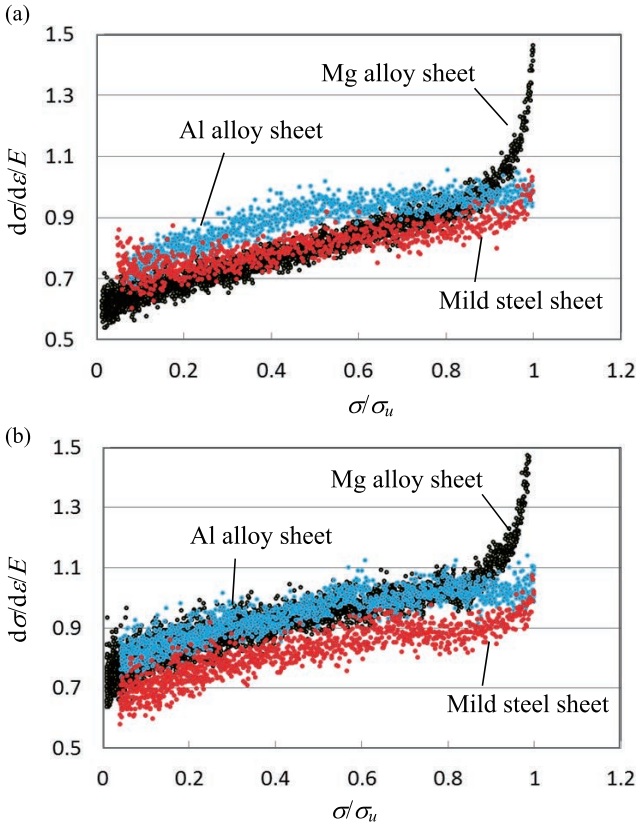

Fig. 5. Variation of instantaneous gradient during unloading at unloaded strains of (a) 0.03 and (c) 0.08. (Online version in color.)

the decrease at small unloaded strains is the largest among the three sheets, whereas the increase at large unloaded strains is larger than that of the Al alloy sheet. The above results describe that the nonlinear behavior during unloading is obviously different depending on the materials.

Figure 5 shows the variations of instantaneous gradient during unloading at unloaded strains of approximately 0.03 and 0.08. The vertical and horizontal axes are normalized using Young's modulus E and the stress at the beginning of unloading, σ_u, respectively. In case of the mild steel sheet, the gradient decreases rapidly at the very beginning of unloading and then it deceases gradually. This tendency is the same as that reported in the literature.[18,20] In case of the Al alloy sheet, such rapid decrease at the beginning hardly occurs and the gradient decreases very gradually from the beginning of unloading. Therefore, the difference in the gradients between the beginning and the end of unloading is smaller in the Al alloy sheet than the mild steel sheet. In case of the Mg alloy sheet, the overall trend is similar to that of the mild steel sheet. On the other hand, the initial rapid decrease is much more pronounced than that in the mild steel sheet, showing that the change in the gradient during unloading is much larger than the other two sheets. The aforementioned characteristics are almost independent of the unloaded strains, but the gradient tends to increase overall in the Mg and Al alloy sheets as the unloaded strain increases.

3.2. Effect of Nonlinearity on Prediction of Strain Recovery

As described in section 3.1, the nonlinearity visually

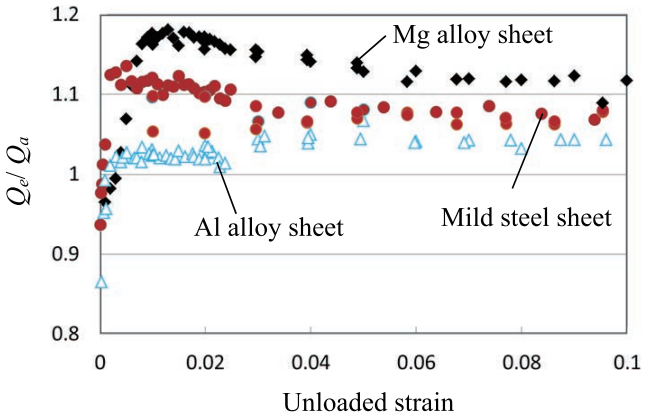

Fig. 6. Variation of energy dissipated during unloading as a function of unloaded strain. (Online version in color.)

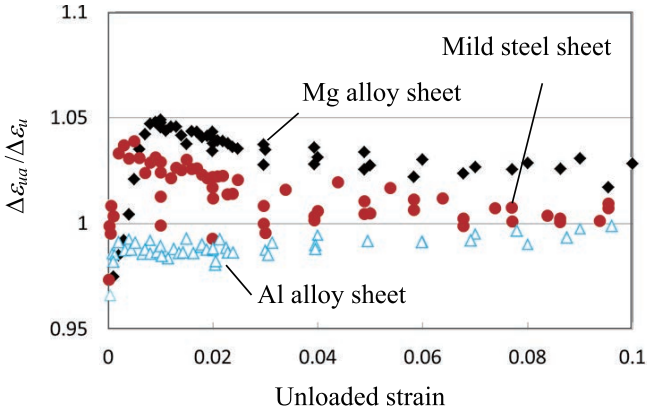

Fig. 7. Variation of ratio $\Delta\varepsilon_{ua}/\Delta\varepsilon_u$ as a function of unloaded strain. (Online version in color.)

observed in the stress-strain curves during unloading (Fig. 2) was more pronounced in the Mg alloy sheet than the mild steel and the Al alloy sheets. On the other hand, the difference in the apparent elastic modulus among the sheets (Fig. 4) was obviously smaller than that expected from the stress-strain curves. For instance, the nonlinearity in the stress-strain curve at an unloaded strain of 0.03 (Fig. 2) is more pronounced in the Mg alloy sheet than that of the mild steel sheet, and this tendency is consistent with the nondimensional energy Q_{ne} (Fig. 3). Conversely, the apparent elastic modulus at an unloaded strain of 0.03 (Fig. 4) in the Mg alloy sheet is as large as that of the mild steel sheet. The above results indicate that the apparent elastic modulus does not always represent the nonlinearity visually observed in the stress-strain curve.

To further examine the relationship between the nonlinearity and the apparent elastic modulus, Fig.6 shows the variations of Q_e/Q_a as a function of unloaded strain where Q_e denotes the energy calculated based on the assumption that the deformation during unloading is perfectly elastic determined by the apparent elastic modulus E_a. The schematic diagram of Q_e is depicted in Fig. 1. If the apparent elastic modulus reflects the nonlinearity during unloading appropriately, the ratio Q_e/Q_a would be close to unity. Conversely, as shown in **Fig. 6**, the ratios are larger than unity irrespective of the materials and their variations are similar to those of the nondimensional energy Q_{ne}. This result displays that the linear approximation of the curve during unloading has a tendency to overestimate the energy dissipated during unloading, which is remarkable when the materials exhibit a strong nonlinearity.

Such error in the energy prediction with use of the linear approximation eventually leads to the error in the amount of strain recovery during unloading. **Figure 7** displays the variations of the ratio between the amount of strain recovery during unloading obtained from the experiment, $\Delta\varepsilon_u$, and that calculated based on the linear elasticity determined by the apparent elastic modulus, $\Delta\varepsilon_{ua}$. $\Delta\varepsilon_u$ and $\Delta\varepsilon_{ua}$ are schematically presented in Fig. 1. The ratio $\Delta\varepsilon_{ua}/\Delta\varepsilon_u$ is very close to unity irrespective of unloaded strain for the Al alloy sheet. On the other hand, the ratio is larger than unity for the mild steel and Mg alloy sheets, indicating that the amount of strain recovery during unloading would be overestimated. This result suggests that, in springback simulations, the simulation accuracy would fall to a low level as the degree of nonlinearity during unloading increases when the apparent elastic modulus is used to model the deformation behavior during unloading. In such a case, it is preferable to employ models that directly take into account the stress-strain curve during unloading such as those proposed by Sun & Wagoner[27] or Andar *et al.*[20]

3.3. Relationship between Nonlinearity and Apparent Elastic Modulus

One of the reasons that the inconsistency between the apparent elastic modulus and the nonlinearity occurred would be the pronounced rapid decrease in the gradient at the beginning of unloading in the Mg alloy and mild steel sheets as shown in Fig. 5. To examine the effect of the initial rapid decrease on the apparent elastic modulus, the following two different definitions of apparent elastic modulus are used: the stress-strain curve was linearly approximated in the stress ranges $0.8 \leq \sigma/\sigma_u \leq 1.0$ and $0.0 \leq \sigma/\sigma_u \leq 0.8$ in the first and second definitions, respectively.

Figure 8 shows the variations of the apparent elastic modulus obtained using the two definitions. When the first definition was used, the apparent elastic moduli are overall larger than those obtained using the original definition (Fig. 4) irrespective of the materials. Conversely, the apparent elastic moduli obtained using the second definition are in good agreement with those of the original definition. The difference in the results between the first and second definitions is the largest in the Mg alloy sheet and it is also large in the mild steel sheet. This tendency is consistent with that of the initial rapid decrease in the gradient (Fig. 5). These results demonstrate that the initial rapid decrease hardly affects the apparent elastic modulus obtained using the original definition, leading to the inconsistency between the apparent elastic modulus and the nonlinearity in the stress-strain curve.

As described earlier, the initial rapid decrease in the gradient was pronounced in the mild steel and Mg alloy sheets, whereas it was hardly observed in the Al alloy sheet. It is recognized that such initial rapid decrease can be explained in terms of the viscoplastic response of the material, *i.e.* the instantaneous reverse movement of the mobile dislocations.[18,22,24] The authors[24] have examined the effect of the strain rate sensitivity exponent on the stress-strain curve during unloading in a Mg alloy sheet using the crystal plasticity finite-element method. It was found that

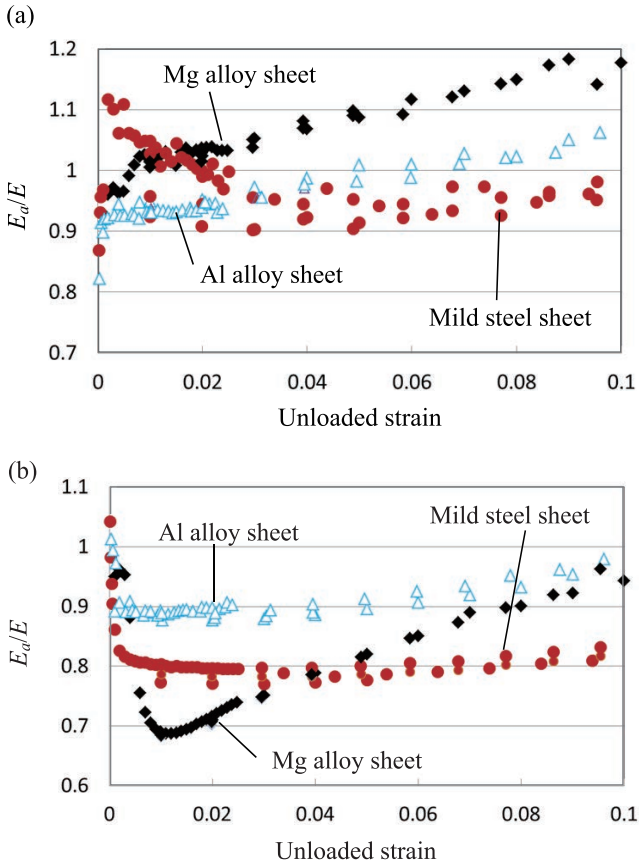

Fig. 8. Apparent elastic modulus obtained from the following two definitions: the stress-strain curve during unloading was linearly approximated in the stress ranges (a) $0.8 \le \sigma/\sigma_u \le 1.0$ and (b) $0.0 \le \sigma/\sigma_u \le 0.8$. (Online version in color.)

the initial rapid decrease does not occur when the strain rate sensitivity exponent is set to nearly zero, whereas it is more pronounced as the strain rate sensitivity exponent becomes large. This result indicates that the strain rate dependency of the materials may be one of the factors that give rise to the difference in the initial rapid decrease among the materials (Fig. 5). From a literature survey, the strain rate sensitivity exponent m for mild steel sheets, AZ31Mg alloy sheets, and 5 000 series Al alloy sheets at room temperature would be respectively within the ranges of approximately $0.02 \le m \le 0.05$,[28–30] $0.01 \le m \le 0.04$,[31–33] and $-0.01 \le m \le 0.005$.[34–36] Clearly, the strain rate sensitivity exponent is larger in the mild steel and Mg alloy sheets than in the Al alloy sheet, consistent with the decreasing tendency at the beginning of unloading.

This result indicates that the deformation during unloading would be notably affected by the strain rate during loading and/or unloading in the mild steel and Mg alloy sheets, whereas it is hardly affected in the Al alloy sheet. Moreover, this result further suggests that the linear approximation of the curve during unloading would not be suitable for materials with a high strain rate sensitivity exponent. It should be noted that there would be other factors that give rise to the initial rapid decrease because the Mg alloy sheet depicts larger decrease than that of the mild steel sheet although the strain rate sensitivity exponent for the Mg alloy sheet is comparable with that of the mild steel sheet. This will be our future work.

4. Crystal Plasticity Finite-Element Analysis

4.1. Crystal Plasticity Finite-Element Method

A crystal plasticity finite-element method is used to investigate the difference in the unloading behavior among the materials from the mesoscopic point of view. Because a crystal plasticity analysis on unloading processes has scarcely been conducted except for our previous works in a Mg alloy sheet,[24,25] the availability of a crystal plasticity analysis on unloading processes in various materials are not understood yet. Therefore, in the present study, the applicability of a crystal plasticity analysis on unloading processes is also discussed.

The crystal plasticity models employed have been used widely in various simulations.[24,25,37–42] Hence, they are explained only briefly here. First the models for the Al alloy (fcc) and mild steel (bcc) sheets are described.[40–42] A family of {111} slip systems and two families of {110} and {112} slip systems are taken into account respectively for fcc and bcc structures. The following visco-plastic power law is used to describe the slip rate $\dot{\gamma}^{(\alpha)}$ of the α slip system

$$\frac{\dot{\gamma}^{(\alpha)}}{\dot{\gamma}_0} = \left|\frac{\tau^{(\alpha)}}{\tau_Y^{(\alpha)}}\right|^{\frac{1}{m}} \mathrm{sign}\left(\tau^{(\alpha)}\right), \dot{\tau}_Y^{(\alpha)} = \sum_\beta q_{\alpha\beta} h \left|\dot{\gamma}^{(\beta)}\right|, \quad \text{..... (2)}$$

where $\tau^{(\alpha)}$ and $\tau_Y^{(\alpha)}$ are Schmid's resolved shear stress and the strength of the α slip system with $\tau_Y^{(\alpha)} = \tau_0$ at the beginning, respectively. τ_0 represents the initial critical resolved shear stress. $\dot{\gamma}_0$ is the reference strain rate, m is the strain rate sensitivity exponent, and $q_{\alpha\beta}$ with $\alpha = \beta$ and with $\alpha \ne \beta$ are the self- and latent- hardening moduli, respectively. For the rate of hardening h, the following law is used

$$h = h_0 \left(\frac{h_0 \bar{\gamma}}{\tau_0 N} + 1\right)^{N-1}, \bar{\gamma} = \sum_\alpha \int \left|\dot{\gamma}^{(\alpha)}\right| \mathrm{d}t, \quad \text{..... (3)}$$

where h_0 and N are the material constants.

For the Mg alloy sheet (hcp), three families of (1000) basal, $\{10\bar{1}0\}$ prismatic, and $\{11\bar{2}2\}$ pyramidal slip systems and a family of $\{10\bar{1}2\}$ twinning systems are taken into consideration.[24,25,37–39] The slip rate $\dot{\gamma}^{(\alpha)}$ is given by Eq. (2). The following two laws are used for the rate of hardening

$$h = h_0 \quad \text{..... (4)}$$

and

$$h = h_0 \left(1 - \frac{\tau_0}{\tau_\infty}\right) \exp\left(-\frac{h_0 \bar{\gamma}}{\tau_\infty}\right), \quad \text{..... (5)}$$

wehre h_0 and τ_∞ are the material constants. Equation (4) is assumed for basal slip, while Eq. (5) is used for prismatic slip and pyramidal slip. For twinning and detwinning, a model originally proposed for the twinning process by Van Houtte[43] and recently extended to the detwinning process by the present authors[25,38] is employed. The hardening of twinning is assumed to obey Eq. (4).

Back stress is not taken into account in the present study because it was depicted in our previous study that the effect of back stress on the unloading behavior in a Mg alloy sheet is negligible.[24]

A finite-element model used was a cube that was divided into 10 uniform eight-node isoparametric brick elements in each direction. Following our previous study,[24,25] dis-

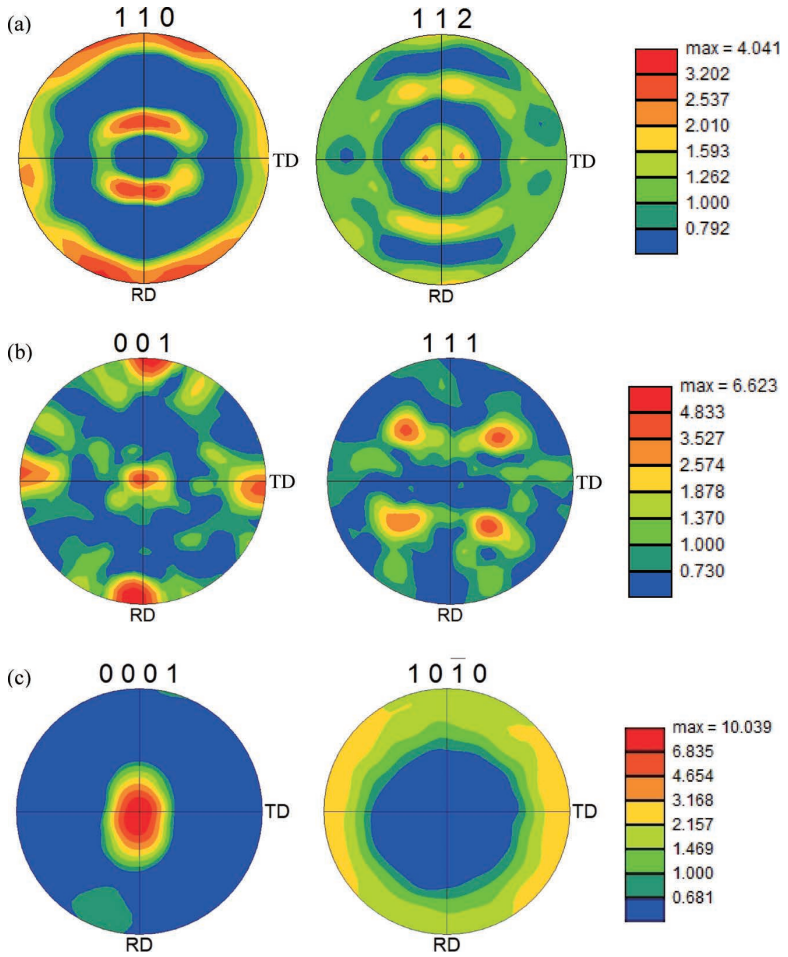

Fig. 9. Initial pole figures of three sheets used in simulations. (a) Mild steel sheet, (b) Al alloy sheet, and (c) Mg alloy sheet. (Online version in color.)

placement increments were imparted to simulate loading-unloading simulations.

Figure 9 displays the initial pole figures of the three sheets measured using electron backscatter diffraction. In the simulations, initial crystallographic orientations were determined based on these results. A same initial orientation was assigned to all eight Gauss integration points in an element for the Mg alloy sheet,[24,25,37,38,44–46] while different initial orientations were assigned to all Gauss integration points for the mild steel and Al alloy sheets.[40–42] Hence, the numbers of initial orientations used in the simulations were 1 000 and 8 000 for hcp and cubic structures, respectively. It should be noted that these numbers are sufficient to examine the deformations up to a strain of approximately 10%.[24]

Isotropic elasticity was assumed and Young's moduli shown in Table 1 were used. Poisson's ratio was set to ν = 0.3 and the reference strain rate to $\dot{\gamma}_0 = 0.001\ \mathrm{s}^{-1}$ for the three sheets. All the components of $q_{\alpha\beta}$ were set to 1 for the mild steel and Al alloy sheets, whereas the parameters presented in the literature[39] were adopted for the Mg alloy sheet. Based on the literature survey discussed in section 3.3, the strain rate sensitivity exponent m was determined to be 0.02, 0.002, and 0.02 for the mild steel, Al alloy, and Mg alloy sheets, respectively.

The Mg alloy sheet was the same as that used in the literature;[45,46] thus, the hardening parameters used in Eqs. (4) and (5) were also the same as those reported in the literature.[45,46] For the mild steel and Al alloy sheets, the hardening parameters employed in Eq. (3) were determined to attain good agreements with experimental stress-strain curves obtained under uniaxial tension at least up to a strain of 10%.

Table 2. Identified parameters for mild steel and Al alloy sheets.

Parameters	Al alloy	Mild steel			
		Case 1		Case 2	
		{110}	{112}	{110}	{112}
τ_0	33	45	45	40	50
h_0	565	965	965	850	850
N	0.35	0.3	0.3	0.3	0.3

In the case of bcc materials, same hardening parameters are usually identified for {110} slip and {112} slip.[e.g.47,48] On the other hand, there are cases where different parameters are employed for the two slip systems[e.g.48,49] and, moreover, {112} slip systems are sometimes not taken into account.[e.g.50,51] In the present study, two sets of parameters were identified for the mild steel sheet to investigate the effect of parameter identification on the simulation result: the parameters for {110} slip and {112} slip were assumed to be the same in case 1, whereas the critical resolved shear stress was assumed to be larger for {112} slip than that of {110} slip in case 2. The identified parameters for the mild steel and Al alloy sheets are shown in **Table 2**. It should be noted that we cannot guarantee the uniqueness of the param-

eters for case 2, *i.e.* multiple sets of parameters that give a similar stress-strain curve under uniaxial tension may exist.

4.2. Simulation Results and Discussion

Figure 10 displays the evolution of the nondimensional energy Q_{ne} obtained from the simulation. The energy increases as unloaded strain increases in the Mg alloy sheet, whereas it is negligibly small in the mild steel and Al alloy sheets. **Figure 11** depicts the variations of apparent elastic modulus. The apparent elastic moduli keep on decreasing as unloaded strain increases within the unloaded strain range examined irrespective of the materials. The amount of decrease is much larger in the Mg alloy sheet than the other two sheets. The results of the mild steel and Al alloy sheets are almost identical. **Figure 12** exhibits the variations of instantaneous gradient at unloaded strains of approximately 0.03 and 0.08. The initial rapid decrease is larger for the mild steel and Mg alloy sheets than the Al alloy sheet because of the larger strain rate sensitivity exponent m for these two materials. In the Mg alloy sheet, the gradient decreases gradually during unloading; thus, the overall decrease in the gradient from the beginning to end of unloading is relatively large. Moreover, it becomes large as the unloaded strain increases. In the Al alloy and mild steel sheets, on the other hand, the gradients remain unchanged during unloading except for the very beginning, but the overall decrease in the gradient becomes large gradually as the unloaded strain increases as in the case of the Mg alloy sheet. These results for the mild steel and Al alloy sheets describe that the stress-strain curves during unloading are almost linear and their slopes become small as the unloaded strain increases. It should be noted that all simulation results for the mild steel sheet are independent of the sets of parameters.

Clearly, the tendencies observed in the Mg alloy sheet are different from those of the mild steel and Al alloy sheets. Comparing the aforementioned simulation results with the experimental results (Figs. 3, 4, and 5), the characteristics that the Mg alloy sheet exhibits a stronger nonlinearity than the other two sheets are in qualitatively good agreement with the experimental results. These results suggest that the stronger nonlinearity observed in the Mg alloy sheet than the mild steel and Al alloy sheets would be because of the hcp structure.

The mechanism that the nonlinearity during unloading under tension in a rolled Mg alloy sheet occurred would be explained as follows.[24] The plastic deformation during tension is primarily governed by the activity of prismatic slip. Because the critical resolved shear stress of basal slip is much smaller than that of prismatic slip, basal slip could be activated during unloading because the stress level during unloading is large enough for basal slip to be activated, yielding the pronounced nonlinearity. This mechanism shows that the difference in the critical resolved shear stress among the slip systems would be one of the causes that the Mg alloy sheet depicts the strong nonlinearity.

If the above mechanism is also applicable to the mild steel sheet, the deformation mechanism should be different between cases 1 and 2. Therefore, the evolution of activity of each family of slip systems,[24,25] r_i, is used to examine the

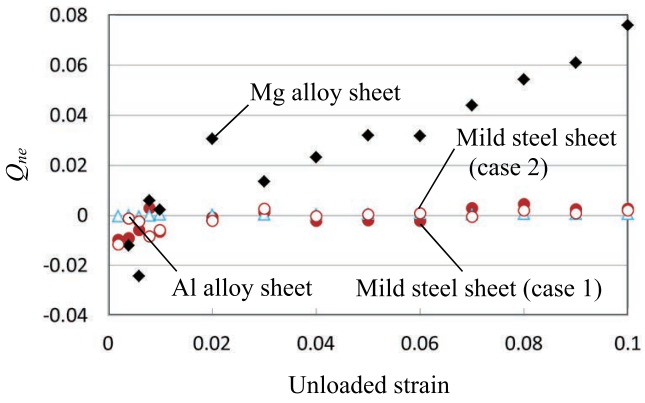

Fig. 10. Evolution of nondimensional energy Q_{ne} obtained from simulations. (Online version in color.)

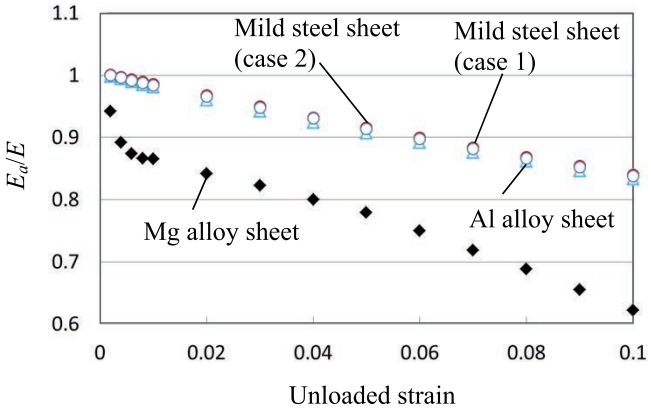

Fig. 11. Variation of apparent elastic modulus obtained from simulations. (Online version in color.)

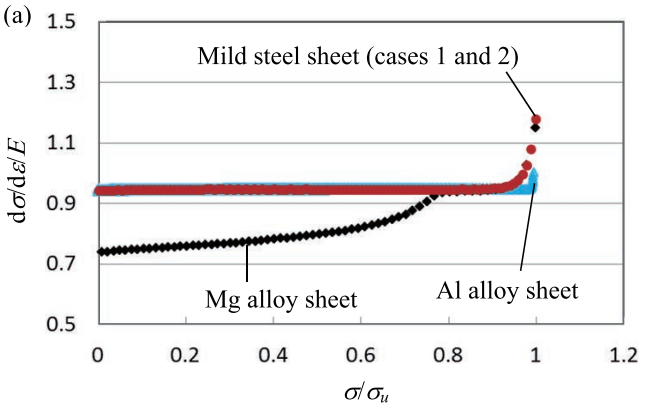

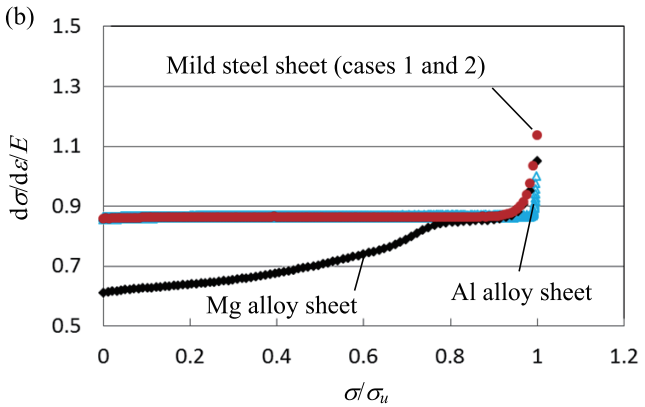

Fig. 12. Variation of instantaneous gradient at unloaded strains of (a) 0.03 and (c) 0.08. (Online version in color.)

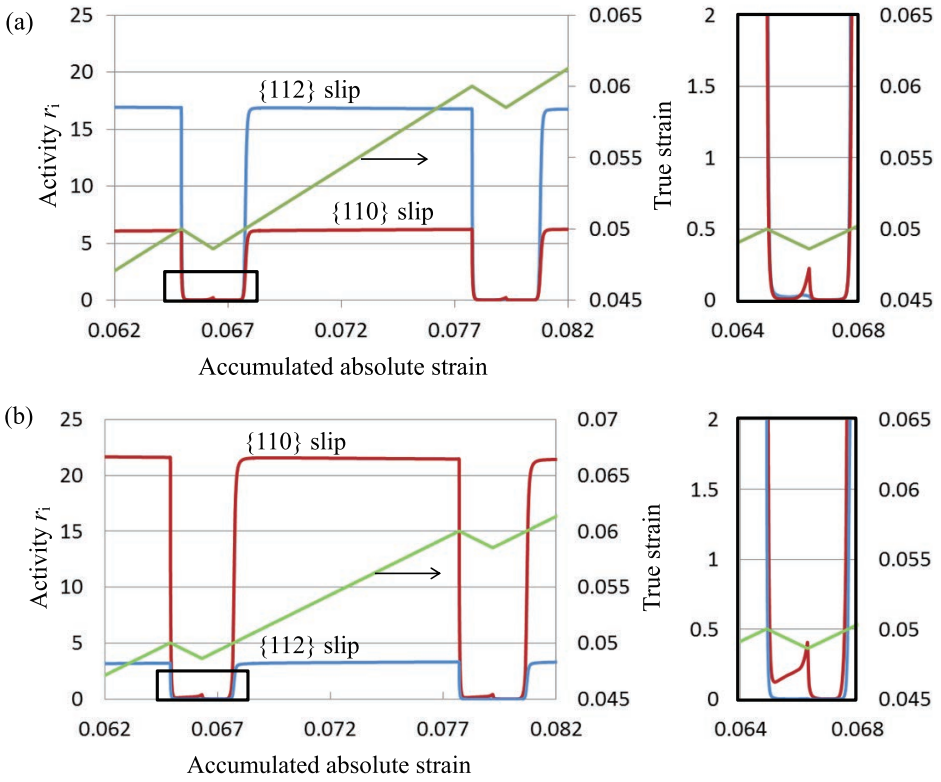

Fig. 13. Evolutions of plastic strain increments in mild steel sheet contributed by families of {110} and {112} slip systems as a function of accumulated absolute strain during loading-unloading. (a) Case 1 and (b) case 2. (Online version in color.)

effect of parameters on the deformation during unloading in the mild steel sheet. The activity r_i is evaluated in the form,

$$r_i = \sum_n \sum_k \left| \Delta\gamma^{(n,k)} \right|, \quad \text{..... (6)}$$

where n and k are the numbers of grains and systems of the family i, respectively. The results for cases 1 and 2 are depicted in **Fig. 13** in which loading-unloading processes at unloaded strains of 0.05 and 0.06 are displayed. Magnified views in the vicinity of unloading designated by the black boxes are also shown on the right hand side. During loading, the activity of {112} slip is larger than that of {110} slip in case 1, whereas the activity of {110} slip is larger than that of {112} slip in case 2. The fact that the activity of {110} slip is larger in case 2 than case 1 is consistent with the parameters. On the other hand, during unloading, the activity of {110} slip is larger than that of {112} slip in both cases and, moreover, the activity of {110} slip is larger in case 2 than case 1. This result indicates that the mesoscopic deformation during unloading is different depending on the sets of parameters and the slip activities tend to increase when different critical resolved shear stresses are identified for {110} slip and {112} slip, consistent with the result of the Mg alloy sheet. The results shown in Figs. 10, 11, and 12 are almost independent of the sets of parameters because the difference in the slip activities may be too small. However, the aforementioned results suggest that the nonlinearity in the mild steel sheet would also be affected by the parameters.

In contrast, the following characteristics observed in the experimental results were not predicted properly in the simulation results. The apparent elastic modulus tends to increase at high unloaded strains in the Al alloy and Mg alloy sheets and it tends to saturate in the mild steel sheet. The instantaneous gradient decreases gradually during unloading; thus, the nondimensional energy Q_{ne} is larger than zero irrespective of the materials. Moreover, the results are different between the Al alloy and mild steel sheets. The discrepancies observed between the experimental and simulation results would describe that, in particular for the cubic structures, other advanced models may be necessary to predict the nonlinearity during unloading. One of the candidates for bcc materials other than the issue of parameters may be the following mechanism. It is well known that in bcc materials the so-called non-Schmid effect is observed. This effect includes several phenomena,[50–52] and one of them is that the slip resistance on {112} slip planes may be different in the twinning and anti-twinning directions.[52] This asymmetry in the slip resistance can increase the nonlinearity during unloading because a similar effect as that the critical resolved shear stresses are different among the slip systems would be expected; thus, the difference in the mesoscopic deformation (Fig. 13) would become larger. Further investigation to increase the simulation accuracy will be performed in future work.

5. Conclusions

The deformation behavior during unloading was examined under uniaxial tension in a mild steel sheet, an aluminum alloy sheet, and a magnesium alloy sheet both experimentally and numerically. The results obtained are summarized as follows.

(1) The nonlinearity during unloading is notably different depending on the materials: it is the largest in the Mg alloy sheet and is larger in the mild steel sheet than the Al

alloy sheet.

(2) The apparent elastic modulus, *i.e.* the linear approximation of the whole stress-strain curve during unloading, decreases as the strain increases to approximately 0.01 irrespective of the materials. On the other hand, at strains larger than approximately 0.01, it tends to saturate in the mild steel sheet, while it tends to increase in the Al alloy and Mg alloy sheets.

(3) The apparent elastic modulus does not always represent the nonlinearity during unloading. More specifically, the linear approximation of the curve during unloading tends to overestimate the amount of strain recovery during unloading, which is remarkable when the materials exhibit a strong nonlinearity. This result indicates that an accuracy of springback simulation would fall to a low level when the apparent elastic modulus is used to model the unloading behavior for materials that exhibit a strong nonlinearity. One of the reasons of this result would be that the difference in the initial rapid decrease in the instantaneous gradient cannot be evaluated properly using the apparent elastic modulus.

(4) The initial rapid decrease in the instantaneous gradient would have a strong correlation with the strain rate sensitivity exponent. This result indicates that the deformation during unloading would be notably affected by the strain rate during loading and/or unloading in the mild steel and Mg alloy sheets, whereas it is hardly affected in the Al alloy sheet. Moreover, this result further suggests that the linear approximation of the curve during unloading would not be suitable for materials with a high rate-sensitivity exponent.

(5) A crystal plasticity analysis demonstrates that one of the reasons that give rise to the nonlinearity during unloading would be the difference in the critical resolved shear stresses among the slip systems. This result is consistent with the fact that the strong nonlinearity is exhibited in the Mg alloy sheet that has the hcp structure. This result further suggests that the parameter identification would affect the simulation results of the mild steel sheet that has the bcc structure. On the other hand, some characteristics observed in the experimental results are not predicted properly in the simulation results, describing that, especially for the bcc and fcc models, other advanced models including the non-Schmid effect may be necessary to predict the unloading behavior. Further investigation to increase the simulation accuracy will be our future work.

Acknowledgments

The authors wish to acknowledge Associate Professor Tsuyoshi Mayama of Kumamoto University, Dr. Tsutomu Tanaka and Dr. Takashi Nishimura of Technology Research Institute of Osaka Prefecture for their help with the EBSD analysis. The authors would like to express their sincere gratitude to UACJ Corporation for providing the sheet material. This research was partially supported by 20th ISIJ research promotion grant and JSPS KAKENHI Grant Number 26289271.

REFERENCES

1) W. D. Carden, L. M. Geng, D. K. Matlock and R. H. Wagoner: *Int. J. Mech. Sci.*, **44** (2002), 79.
2) F.-K. Chen and T.-B. Huang: *J. Mater. Process. Technol.*, **142** (2003), 643.
3) K. Mori, K. Akita and Y. Abe: *Int. J. Mach. Tool. Manuf.*, **47** (2007), 321.
4) T. Hama, Y. Kariyazaki, K. Ochi, H. Fujimoto and H. Takuda: *Mater. Trans.*, **51** (2010), No. 4, 685.
5) R. H. Wagoner, H. Lim and M. G. Lee: *Int. J. Plast.*, **45** (2013), 3.
6) T. Geka, M. Asakura, T. Kiso, T. Sugiyama, M. Takamura and M. Asakawa: *Key Eng. Mater.*, **554–557** (2013), 1320.
7) A. P. Karafillis and M. C. Boyce: *Int. J. Mach. Tool. Manuf.*, **36** (1996), 503.
8) K. P. Li, W. P. Carden and R. H. Wagoner: *Int. J. Mech. Sci.*, **44** (2002), 103.
9) M. C. Oliveira, J. L. Alves, B. M. Chaparro and L. F. Menezes: *Int. J. Plast.*, **23** (2007), No. 3, 516.
10) R. H. Wagoner and M. Li: *Int. J. Plast.*, **23** (2007), No. 3, 345.
11) T. Hama, T. Nagata, C. Teodosiu, A. Makinouchi and H. Takuda: *Int. J. Mech. Sci.*, **50** (2008), No. 2, 175.
12) M. Banu, M. Takamura, T. Hama, O. Naidim, C. Teodosiu and A. Makinouchi: *J. Mater. Process. Technol.*, **173** (2006), No. 2, 178.
13) T. Kuwabara: *Int. J. Plast.*, **23** (2007), No. 3, 385.
14) D. Banabic, H. Aretz, D. S. Comsa and L. Paraianu: *Int. J. Plast.*, **21** (2005), No. 3, 493.
15) F. Yoshida and T. Uemori: *Int. J. Plast.*, **18** (2002), No. 5,6, 661.
16) F. Barlat, J. J. Gracio, M. G. Lee, E. F. Rauch and G. Vincze: *Int. J. Plast.*, **27** (2011), No. 9, 1309.
17) R. K. Verma, K. Chung and T. Kuwabara: *ISIJ Int.*, **51** (2011), No. 3, 482.
18) R. M. Cleveland and A. K. Ghosh: *Int. J. Plast.*, **18** (2002), 769.
19) L. Guo and A. K. Ghosh: *J. Eng. Mater. Technol. ASME*, **125** (2003), 237.
20) M. O. Andar, T. Kuwabara, S. Yonemura and A. Uenishi: *ISIJ Int.*, **50** (2010), 613.
21) H. Kim, C. Kim, F. Barlat, E. Pavlina and M. G. Lee: *Mater. Sci. Eng. A*, **562** (2013), 161.
22) H. Hamasaki, Y. Hattori, K. Furukawa and F. Yoshida: *Procedia Eng.*, **81** (2014), 969.
23) T. Hama, K. Ochi, N. Kitamura, H. Fujimoto and H. Takuda: *Steel Res. Int.*, Special Edition, (2011), 1054.
24) T. Hama and H. Takuda: *Int. J. Plast.*, **27** (2011), 1072.
25) T. Hama, N. Kitamura and H. Takuda: *Mater. Sci. Eng. A*, **583** (2013), 232.
26) L. Sun and R. H. Wagoner: *Int. J. Plast.*, **27** (2011), 1126.
27) F. Yoshida, T. Uemori and K. Fujiwara: *Int. J. Plast.*, **18** (2002), 633.
28) P. Larour, A. Bäumer, K. Dahmen and W. Bleck: *Steel Res. Int.*, **84** (2013), 426.
29) H. B. Sun, F. Yoshida, M. Ohmori and X. Ma: *Mater. Lett.*, **57** (2003), 4535.
30) A. Askariani, R. Mahmudi and M. H. Pishbin: *Steel Res. Int.*, **81** (2010), 1097.
31) O. Duygulu and S. R. Agnew: Magnesium Technology 2003, TMS, Warrendale, PA, (2003), 237.
32) X. Z. Lin and D. L. Chen: *J. Mater. Eng. Perform.*, **17** (2008), 894.
33) H. Nishimura, O. Hasegawa, N. Koiso and K. Matsumoto: *J. Jpn Inst. Light Met.*, **53** (2003), 302.
34) R. C. Picu, G. Vincze, F. Ozturk, J. J. Gracio, F. Barlat and A. M. Maniatty: *Mater. Sci. Eng. A*, **390** (2005), 334.
35) F. Ozturk, H. Pekel and H. S. Halkaci: *J. Mater. Eng. Perform.*, **20** (2011), 77.
36) O. Noguchi: *Furukawa-Sky Rev.*, **3** (2007), 1.
37) T. Hama and H. Takuda: *Comput. Mater. Sci.*, **51** (2012), 156.
38) T. Hama and H. Takuda: *Steel Res. Int.*, Special Edition, (2012), 1115.
39) S. Graff, W. Brocks and D. Steglich: *Int. J. Plast.*, **23** (2007), 1957.
40) E. Nakamachi, C. L. Xie and M. Harimoto: *Int. J. Mech. Sci.*, **43** (2001), 631.
41) E. Nakamachi, C. L. Xie, H. Morimoto, K. Morita and N. Yokohama: *Int. J. Plast.*, **18** (2002), 617.
42) C. L. Xie and E. Nakamachi: *Mater. Sci. Eng. A*, **340** (2003), 130.
43) P. Van Houtte: *Acta Metall.*, **26** (1978), 591.
44) T. Hama, N. Hosokawa and H. Takuda: Proc. NUMISHEET 2014, ed. by J. W. Yoon, B. Rolfe, J. H. Beynon and P. Hodgson, AIP Publishing, New York, (2014), 692.
45) T. Hama, T. Mayama and H. Takuda: *Key Eng. Mater.*, **611–612** (2014), 27.
46) T. Hama and H. Takuda: *Key Eng. Mater.*, **622–623** (2014), 603.
47) R. K. Verma, A. Kumar, G. Manikandan and T. Kuwabara: *Mater. Sci. Eng. A*, **559** (2013), 359.
48) K. Kitayama, C. N. Tome, E. F. Rauch, J. J. Gracio and F. Barlat: *Int. J. Plast.*, **46** (2013), 54.
49) K. Kitayama, T. Kobayashi, T. Uemori and F. Yoshida: *ISIJ Int.*, **52** (2012), 735.
50) C. R. Weinberger, C. C. Battaile, T. E. Buchheit and E. A. Holm: *Int. J. Plast.*, **37** (2012), 16.
51) A. Patra, T. Zhu and D. L. McDowell: *Int. J. Plast.*, **59** (2014), 1.
52) T. Yalcinkaya, W. A. M. Brekelmans and M. G. D. Geers: *Modelling Simul. Mater. Sci. Eng.*, **16** (2008), 085007.